Dynamic Loads Due to Wind Shear

BRUCE E CLINGAN*
The Boeing Company, Seattle, Wash

An analytical study of dynamic loads induced by wind shear is reported In the first portion of the study, the effect of simplifications in the equations of motion on solution accuracy is investigated Pitch-plane wind-shear bending moments on a hypothetical boost-glide vehicle are determined using three methods In the first method the equations used are only partially linearized, and the vehicle follows the programmed trajectory by responding to the thrust vectoring control Varying parameters are functions of computed altitude, computed Mach number, or time as appropriate In the second method linearized perturbation equations are used, and all parameters are considered functions of time based on the nominal no-wind trajectory In the third method quasi-steady pitching and bending are assumed Comparisons of bending moment time histories obtained using each of the three methods are shown Significant errors may occur when the perturbation or quasi-steady equations are used In the second part of the study, the influence of a number of major parameters on wind-shear loads is investigated These include fineness ratio, structural stiffness, mass distribution, payload lifting area, tail fin area, control law, and initial thrust to weight ratio

Nomenclature

a = speed of sound
BM_j = bending moment at $x = x_j$
C_A = axial force coefficient
$C_{N_{\alpha i}}$ = local normal force derivative for ith element
g = acceleration of gravity
h = altitude
I = pitching moment of inertia
K_α = angle of attack feedback gain
K_θ = attitude feedback gain
$K_{\dot\theta}$ = rate feedback gain
M = Mach number
m = vehicle mass
m_1 = generalized mass for bending mode
m_i = mass of ith element
m_0 = initial mass
m_r = mass rate of flow
q_T = translation normal to the flight path
q_θ = perturbation pitch attitude
S = glider area
S_e = nozzle exit area
S_i = area of ith element
T = thrust
T_0 = sea level thrust
U = component of vehicle velocity in the x direction
U_0 = forward velocity for nominal no-wind trajectory
V = velocity of vehicle relative to air
V_w = horizontal wind velocity
w = component of vehicle velocity in the z direction
x_i = x coordinate of ith station, positive forward of cg
x_j = x coordinate of jth bending moment station
x_T = x coordinate of nozzle hinge point
x_α = x coordinate of angle of attack sensor
δ = nozzle gimbal angle
ζ_1 = damping ratio for bending mode
θ = pitch attitude
θ_0 = pitch attitude for the nominal no-wind trajectory
θ_p = programmed pitch attitude
ξ = generalized coordinate for bending mode
ρ = air density
ϕ_A' = slope at attitude sensor location [body station (B S) 411]
ϕ_i = modal value at $x = x_i$
ϕ_i' = slope at $x = x_i$
ϕ_j = modal value at $x = x_j$
ϕ_R' = slope at rate sensor location (B S 1636)
ϕ_T = modal value at nozzle hinge point
ϕ_T' = slope at nozzle hinge point
ϕ_α = modal value at angle of attack sensor location (B S 0)
ϕ_α' = slope at angle of attack sensor location
ω_1 = frequency of bending mode

Presented as Preprint 63-207 at the AIAA Summer Meeting in Los Angeles, Calif , June 17–20, 1963; revision received October 31, 1963 This paper includes research efforts supported by the Aeronautical Systems Division, Air Force Systems Command, U S Air Force, under Contract AF 33(657)-8808 [1]

* Research Specialist, Aero Space Division Member AIAA

Introduction

DURING boost, rocket-propelled vehicles are subjected to the axial loads of thrust and drag, and to bending loads produced by wind shear, atmospheric turbulence, and maneuver The bending loads are likely to be critical for vehicles with winged payloads, and wind shear generally produces the largest bending loads The purpose of this study was to examine the accuracy of several analytical methods for predicting wind-shear loads on boost-glide vehicles, and to investigate the influence of some parameter changes on wind-shear loads

The state of the art in the analysis of airplane gust loads was highly refined at the time wind shear became important as a load producing environment The similarity between a horizontally flying airplane encountering a vertical gust and a vertically rising vehicle encountering wind shear was immediately recognized, and it was only natural that the wind-shear problem should be treated by some investigators as a type of gust loads problem The equations of motion for perturbation from a nominal no-wind trajectory were similar to those used for gust-loads analysis except for the time varying coefficients The use of perturbation equations was based on certain small angle assumptions as well as the assumption that wind-caused deviations from the nominal altitude and forward velocity time histories would not significantly affect wind-shear loads solutions The advantage in using perturbation equations was that the equations could be linearized and the number of rigid body degrees of freedom could be reduced The small angle assumptions appeared to be well founded, but the effect of neglecting wind-caused deviations in the trajectory needed investigating in the case of pitch-plane winds

In addition to the need for evaluation and improvement of the regular dynamic loads analysis methods, quick preliminary design methods were needed for all loading conditions, particularly wind shear, which was found to produce much more severe bending loads than gusts Efforts to reduce the time required for preliminary design loads analysis led to the development of the quasi-steady method described in Ref 2

In some cases this method was found to yield remarkably accurate results However, further studies were required to determine some of the limitations of the method

Finally, since wind-shear bending loads were found to be extremely significant in the design of boost glide type vehicles, a study of the influence of variations in the major parameters was needed to establish trends that might be useful in minimizing wind-shear loads in the design of vehicles of this type

Evaluation of Analysis Methods

Methods Examined

The objective of this portion of the study was to evaluate the accuracy of three analytical methods for determining dynamic loads due to wind shear Since the vehicles being analyzed had winged payloads, only pitch-plane wind profiles and pitch-plane response were considered All three of the methods examined involved solving equations of motion and bending moment equations for time histories of bending moment due to flight through a particular wind profile The difference in the methods lay in the degree of simplification of the equations of motion

The effects of a number of simplifications frequently employed in wind-shear loads analysis were investigated in Ref 3 It was found that engine inertia and liquid slosh could safely be neglected in the prediction of wind-shear loads, although not in the study of dynamic stability It was also found that the response of the flexible modes to wind shear was nearly quasi-static and that a relatively small number of flexible modes were required to represent adequately the elastic response of the structure Therefore, engine inertia and liquid slosh were neglected in this investigation, and only one flexible mode was included

In the first method the equations of motion were only partially linearized Degrees of freedom, referred to body axes, included translation in two directions, pitch, and bending in the first normal mode The vehicle followed a programmed trajectory by responding to thrust vectoring control, and varying parameters were functions of computed altitude, computed Mach number, or time, as appropriate The horizontal wind velocity was resolved into components parallel and perpendicular to the computed pitch attitude, and small gimbal angles were not assumed Solutions for wind-shear loads obtained using the nonlinear equations were referred to as nonlinear solutions, and these were considered as the standards for comparison in evaluating the accuracy of the other two methods

In the second method linearized perturbation equations were used These equations were derived from the nonlinear equations In the perturbation equations a forward translation degree of freedom was not included All parameters were treated as functions of time, based on the nominal no-wind trajectory The horizontal wind was resolved into components parallel and perpendicular to the nominal pitch attitude, and small gimbal angles were assumed The perturbation equations were completely linear and included one less degree of freedom than the nonlinear equations

In the third method quasi-steady pitching and bending were assumed The quasi-steady equation of motion was derived from the perturbation equations as shown in Ref 2 The response was defined in terms of a single degree of freedom, translation normal to the flight path Constant coefficients and linear forcing functions were assumed within small altitude bands so that solutions could be obtained by Laplace transforms The principal application of this extremely simplified method has been in computing statistical distributions of maximum wind-shear loads due to a large sample of measured wind profiles The quasi-steady method is the only one of the three considered which could be used without a computer if necessary

Equations of Motion

The nonlinear equations of motion used in the analysis are given:

$$\dot{U} + w\dot{\theta} = -g\sin\theta + \frac{T}{m}\cos(\delta - \phi_T'\xi) - \frac{\rho V^2}{2m}C_A S \quad (1)$$

$$\dot{w} - U\dot{\theta} = g\cos\theta - \frac{T}{m}\sin(\delta - \phi_T'\xi) - \frac{\rho V}{2m}\left[\sum_i C_{N\alpha_i} S_i(w + V_w\sin\theta) - \sum_i C_{N\alpha_i} S_i x_i\dot{\theta} + \sum_i C_{N\alpha_i} S_i\phi_i\dot{\xi} - V\sum_i C_{N\alpha_i} S_i\phi_i'\xi\right] \quad (2)$$

$$\ddot{\theta} = \frac{T}{I}[x_T\sin(\delta - \phi_T'\xi) + \phi_T\xi\cos(\delta - \phi_T'\xi)] + \frac{\rho V}{2I}\left[\sum_i C_{N\alpha_i} S_i x_i(w + V_w\sin\theta) - \sum_i C_{N\alpha_i} S_i x_i^2\dot{\theta} + \sum_i C_{N\alpha_i} S_i x_i\phi_i\dot{\xi} - V\sum_i C_{N\alpha_i} S_i x_i\phi_i'\xi\right] \quad (3)$$

$$m_1(\ddot{\xi} + 2\zeta_1\omega_1\dot{\xi} + \omega_1^2\xi) = -T\phi_T\sin(\delta - \phi_T'\xi) - \frac{\rho V}{2}\left[\sum_i C_{N\alpha_i} S_i\phi_i(w + V_w\sin\theta) - \sum_i C_{N\alpha_i} S_i\phi_i x_i\dot{\theta} + \sum_i C_{N\alpha_i} S_i\phi_i^2\dot{\xi} - V\sum_i C_{N\alpha_i} S_i\phi_i\phi_i'\xi\right] \quad (4)$$

Engine gimbal angle was governed by the following general relationship:

$$\delta = K_\theta(\theta - \theta_P - \phi_A'\xi) + K_{\dot\theta}(\dot{\theta} - \phi_R'\dot{\xi}) + K_\alpha\left(\frac{w + V_w\sin\theta - x_\alpha\dot{\theta} + \phi_\alpha\dot{\xi}}{V} - \phi_\alpha'\xi\right) \quad (5)$$

Particular control laws were obtained by assigning appropriate values to the gain settings.

Since the wind profile and atmospheric properties were functions of altitude, the following equation relating altitude to the body coordinates was needed:

$$\dot{h} = U\sin\theta - w\cos\theta \quad (6)$$

Density, thrust, and the sonic speed were expressed as functions of altitude based on a standard atmosphere For altitudes less than 35,332 ft

$$\rho = 0.002378(1 - 0.000006879h)^{4.2611} \quad (7)$$

$$T = T_0 + S[2116 - 2116(1 - 0.000006879h)^{5.2611}] \quad (8)$$

$$a = (1244600 - 8.5619h)^{1/2} \quad (9)$$

For altitudes above 35,332 ft

$$\rho = 0.0007265e^{(1.6867 - 0.0004774h)} \quad (10)$$

$$T = T_0 + S[2116 - 489.64e^{(1.6867 - 0.0004774h)}] \quad (11)$$

$$a = 970.93 \quad (12)$$

Relative velocity and Mach number were computed as follows:

$$V = U + V_w\cos\theta \quad (13)$$

$$M = V/a \quad (14)$$

The total mass of the vehicle was assumed to vary linearly with time:

$$m = m_0 + m_r t \quad (15)$$

Variable parameters other than those defined by one of the above equations were tabulated vs altitude, Mach number,

or time, as appropriate; and the digital program performed linear interpolations as necessary Parameters that were functions of both time and Mach number, such as $\Sigma C_{N_{\alpha_i}} S_i \phi_i$, for example, were treated as functions of Mach number

Bending moment was computed according to the following equation, based on force summation:

$$BM_j = (\rho V/2)[\Sigma C_{N\alpha_i} S_i(x_i - x_j)(w + V_w \sin\theta) - \Sigma C_{N\alpha_i} S_i x_i(x_i - x_j)\dot{\theta} + \Sigma C_{N\alpha_i} S_i \phi_i(x_i - x_j)\dot{\xi} - V\Sigma C_{N\alpha_i} S_i \phi_i'(x_i - x_j)\xi] + \Sigma(x_i - x_j)m_i \times (\dot{w} - U\dot{\theta} - g\cos\theta) - \Sigma(x_i - x_j)m_i x_i \ddot{\theta} + \Sigma(x_i - x_j)m_i \phi_i \ddot{\xi} - \Sigma(\phi_i - \phi_j)m_i(T/m)\xi \quad (16)$$

The summations in Eq 16 were over the stations forward of x_j

The perturbation equations of motion, derived from the nonlinear equations, were as follows:

$$\dot{w} - U_0\dot{q}_\theta = -g\sin\theta_0 q_\theta - \frac{T}{m}(\delta - \phi_T'\xi) - \frac{\rho V}{2m} \times \left[\sum_i C_{N\alpha_i} S_i(w + V_w \sin\theta_0) - \sum_i C_{N\alpha_i} S_i x_i \dot{q}_\theta + \sum_i C_{N\alpha_i} S_i \phi_i \dot{\xi} - V\sum_i C_{N\alpha_i} S_i \phi_i'\xi\right] \quad (17)$$

$$\ddot{q}_\theta = \frac{T}{I}[x_T(\delta - \phi_T'\xi) + \phi_T\xi] + \frac{\rho V}{2I} \times \left[\sum_i C_{N\alpha_i} S_i x_i(w + V_w \sin\theta_0) - \sum_i C_{N\alpha_i} S_i x_i^2 \dot{q}_\theta + \sum_i C_{N\alpha_i} S_i x_i \phi_i \dot{\xi} - V\sum_i C_{N\alpha_i} S_i x_i \phi_i'\xi\right] \quad (18)$$

$$m_1(\ddot{\xi} + 2\zeta_1\omega_1\dot{\xi} + \omega_1^2\xi) = -T\phi_T(\delta - \phi_T'\xi) - \frac{\rho V}{2} \times \left[\sum_i C_{N\alpha_i} S_i \phi_i(w + V_w \sin\theta_0) - \sum_i C_{N\alpha_i} S_i \phi_i x_i \dot{q}_\theta + \sum_i C_{N\alpha_i} S_i \phi_i^2 \dot{\xi} - V\sum_i C_{N\alpha_i} S_i \phi_i \phi_i'\xi\right] \quad (19)$$

where

$$\delta = K_\theta(q_\theta - \phi_A'\xi) + K_{\dot{\theta}}(\dot{q}_\theta - \phi_R'\dot{\xi}) + K_\alpha\left(\frac{w + V_w \sin\theta_0 - x_\alpha\dot{q}_\theta + \phi_\alpha\dot{\xi}}{V} - \phi_\alpha'\xi\right) \quad (20)$$

$$V = U_0 + V_w \cos\theta_0 \quad (21)$$

$$\theta = \theta_0 + q_\theta \quad (22)$$

The equation for bending moment was also modified in accordance with the assumptions used in deriving the perturbation equations of motion

The quasi-steady equations for the kth time interval were as follows:

$$\ddot{q}_T + A_k\dot{q}_T = A_k[a_k + b_k(t - t_{k-1})] \quad (23)$$

$$BM_j = B_{jk}[a_k + b_k(t - t_{k-1}) + \dot{q}_T] + C_{jk}\ddot{q}_T \quad (24)$$

where A_k, B_{jk}, and C_{jk} were functions of the average values of the vehicle and trajectory parameters within the kth time interval, and a_k and b_k were constants defining the wind forcing function within the kth time interval The quasi-steady equations were derived from the perturbation equations by first making the transformation $\dot{q}_T = w - U_0\dot{q}_\theta$ and then assuming that $\dot{q}_\theta = \ddot{q}_\theta = \dot{\xi} = \ddot{\xi} = 0$ Details of the derivation and formulas for evaluating the coefficients are given in Ref 2

Solutions of these equations were evaluated at a sufficient number of time points to define the time history of bending moment

Results

It was assumed that the nonlinear equations yielded the most accurate bending moment solutions, since the perturbation and quasi-steady equations represented further simplifications of the nonlinear equations The approach used was to obtain time histories of bending moment due to boost through a given wind profile using each of the three methods and to compare the results The nonlinear solution was used as a standard for evaluating the accuracy of the other two

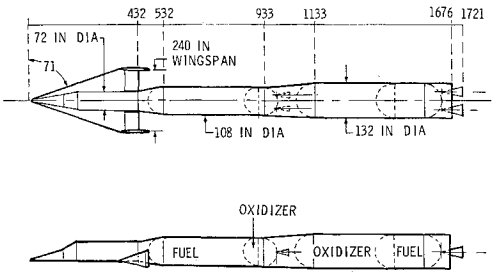

Fig 1 Nominal configuration

The vehicle analyzed is described in Ref 3 and illustrated in Fig 1, and the wind profile used is shown in Fig 2 The nominal no-wind trajectory was a typical gravity turn, experiencing a maximum dynamic pressure of 957 psf at 36,100 ft The wind profile was assumed to lie in the plane of the trajectory, oriented so as to produce a headwind condition

The first solution obtained with the nonlinear equations was a no-wind solution The no-wind case was run in order to 1) determine the no-wind angle of attack and gimbal angle, and 2) determine how closely the nominal no-wind trajectory was followed by the vehicle having pitch inertia and controlled to follow a pitch program by a feedback control system The agreement was remarkably good Pitchover transients died out quickly, and for all practical purposes the vehicle followed the nominal, no-wind trajectory for the remainder of the flight

After obtaining the no wind solution, the solutions for windshear bending moment were obtained using the three methods It was expected that the agreement between the various solutions would be influenced to some extent by variations in control parameters, particularly in the case of the quasi-steady method For example, it was expected that incorporating an angle of attack feedback in the control system would have an important effect on the accuracy of the quasi-steady method

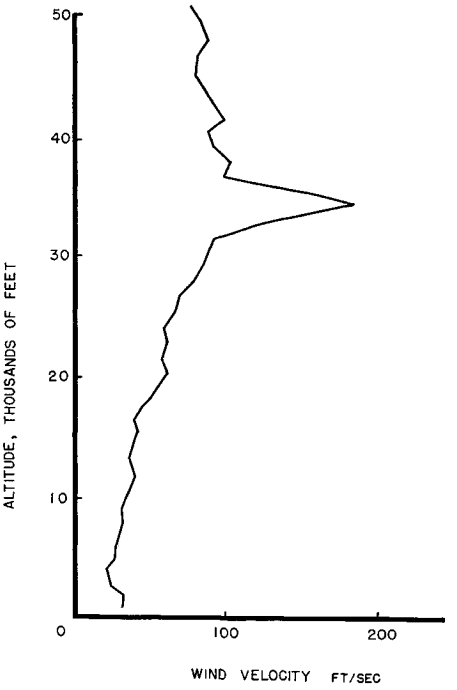

Fig 2 Wind profile, January 3, 1958, Montgomery, Ala

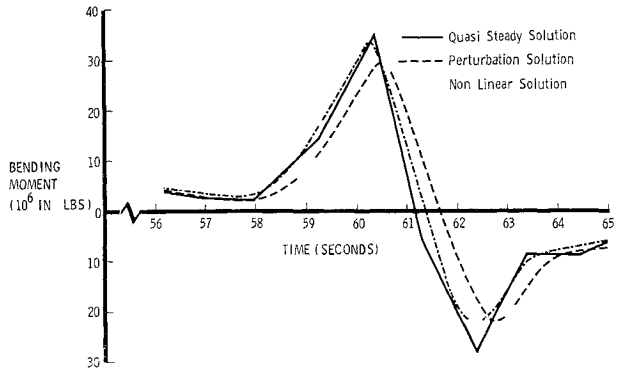

Fig 3 Comparison of solutions for wind-shear loads with the attitude control law

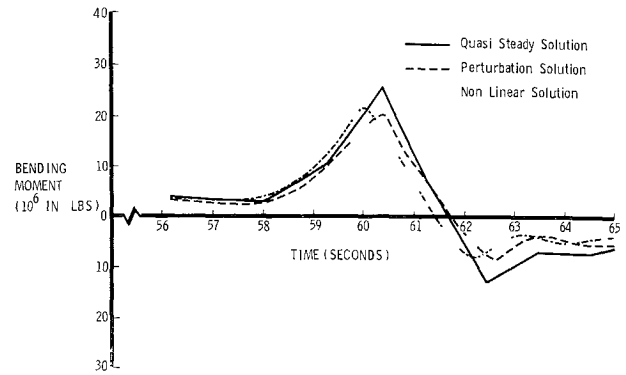

Fig 4 Comparison of solutions for wind-shear loads with neutral static stability control law

Obviously, a vehicle having a pure angle of attack feedback ($K_\theta = 0$) would experience zero wind-shear loads under the quasi-steady assumptions, although in actuality quite large angles of attack and loads could result from dynamic effects Therefore, comparisons of wind-shear loads solutions using the three methods were obtained with several control laws In these variations control law was determined by the relative magnitudes of the attitude and angle of attack feedback gains K_θ and K_α, and the pitch frequency was determined by the sum of these gains Three control laws were used: the attitude law, a neutral static stability, and the minimum drift law [4]

In the first comparison the attitude control law was used, i e , the angle of attack feedback gain was zero ($K_\alpha = 0$) The attitude and rate gains were continuously varied to maintain an undamped pitch frequency of 0 5 cps and 0 6 critical damping throughout boost, based on the nominal trajectory conditions The results are shown in Fig 3, in which time histories of bending moment for the critical booster station are compared It is seen that the time histories are generally similar in appearance, but there are noticeable differences in the maximum predicted bending moments In this case, the perturbation solution underestimated the maximum load by about 12%, whereas the quasi-steady method overestimated the maximum by 6 2% Examination of Fig 3 also reveals that the perturbation and quasi-steady solutions show the maximum load occurring at a slightly later time than in the nonlinear solution This is because the vehicle was blown above the nominal trajectory by the wind, thereby reaching the altitude of the wind spike sooner than in the no wind case, despite a reduction in forward velocity due to the headwind component This effect was not accounted for in the perturbation and quasi-steady solutions, in which the wind velocity and all parameters were considered functions of time, based on the nominal no-wind trajectory

In the second comparison a so-called neutral static stability control law was used In this control law the angle of attack feedback gain is made just large enough to simulate neutral static stability The angle of attack feedback causes the vehicle to respond as if it had tail fins, and it is possible to calculate the gain required to simulate the neutral static stability condition The angle of attack gain which would produce zero pitch frequency by itself was computed, and then the attitude gain was set to bring the sum of K_θ and K_α up to a value corresponding to the 0 5 cps pitch frequency The gains were varied with time to maintain this condition throughout boost A comparison of bending moment time histories ob tained using each of the three solution methods with the neutral static stability control law is shown in Fig 4 The results are generally similar to those obtained with the attitude control law In this case the maximum load was overestimated by 17 4% in the quasi-steady solution and underestimated by 7 8% in the perturbation solution Although the quasi-steady solution gave a rather crude estimate of the maximum load in this case, the time history was generally similar to the nonlinear solution The quasi-steady method would probably be adequate for identifying the most severe profiles out of a large sample of measured profiles The small amount of angle of attack feedback employed in the neutral static stability control law apparently does not invalidate the method in this case

In the third comparison, the minimum drift control law was employed In this control law the attitude and angle of at tack gains were proportioned to produce a minimum drift response according to the method presented in Ref 4 and extended in Ref 5 to account for bending deflections in the calculations of the gains Application of the minimum drift law resulted in considerably higher values of K_α than the neutral static stability law, as shown in Table 1 As in the previous comparisons, the sum of K_θ and K_α was chosen to give an undamped pitch frequency of 0 5 cps throughout boost, and the rate gain $K_{\dot\theta}$ was chosen to maintain 0 6 critical damping Figure 5 shows the comparison of the time histories of bending moment experienced with the minimum drift control law In this case the perturbation and quasi-steady solutions underestimated maximum load by 6 5 and 34%, re spectively It is seen that, although the perturbation solution exhibits the same general appearance as the nonlinear solution, the quasi-steady solution shows very poor agreement The negative peak appearing in the nonlinear and perturbation solutions is not predicted at all by the quasi-steady method Thus, it appears that the quasi-steady method is not applicable in cases where a large amount of angle of attack feedback

Table 1 Gain settings

	Attitude law			Neutral static stability law			Minimum drift law		
Time	K_θ	$K_{\dot\theta}$	K_α	K_θ	$K_{\dot\theta}$	K_α	K_θ	$K_{\dot\theta}$	K_α
0	3 097	1 375	0	3 097	1 375	0 000	3 097	1 375	0 000
18	3 305	1 254	0	2 959	1 254	0 325	1 889	1 254	1 330
30	3 950	1 199	0	2 775	1 199	1 033	0 921	1 199	2 722
42	4 885	1 211	0	2 516	1 211	2 062	0 417	1 211	3 894
54	5 385	1 270	0	2 314	1 270	2 594	0 263	1 270	4 329
66	4 891	1 228	0	2 203	1 228	2 298	0 294	1 228	3 932
78	3 901	1 087	0	2 112	1 087	1 582	0 439	1 087	3 068

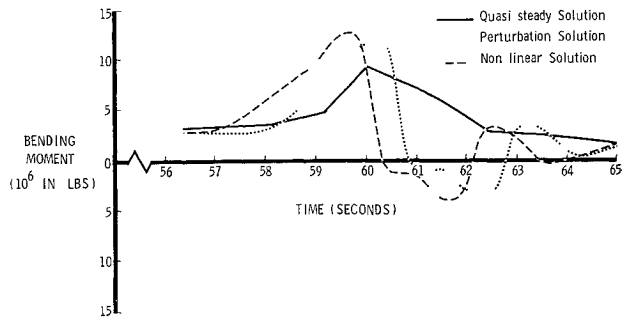

Fig 5 Comparison of solutions for wind shear loads with minimum drift control law

is employed in the control system It should be pointed out that the poor agreement shown in this case is a result of the quasi-steady pitching assumption The nonvibratory character of the nonlinear and perturbation solutions in Figs 3–5 indicates that the assumption of quasi-steady bending is valid

The errors in the bending moments predicted by the perturbation and quasi-steady solutions might be either larger or smaller for other vehicles and other wind profiles In Ref 1 a comparison of rigid body angle of attack time histories in response to the 1959 Sissenwine wind profile[6] was made in which the maximum angle of attack is underestimated by 16 4% in the perturbation solution

For the perturbation solutions, the bending moment errors in Figs 3–5 varied from 6 5 to 12% These errors, although not exceedingly large, were considered too large to ignore in the prediction of design loads Therefore, the nonlinear equations were used in the parameter studies that followed The quasi-steady solutions were sufficiently accurate for preliminary design loads estimates in the first and possibly the second case, but not in the third case where a large angle of attack feedback was employed

Parameter Variation Studies

In this portion of the study the major parameters were varied in order to determine the influence of parameter changes on dynamic loads The purpose was to establish trends that may be useful in the design of boost-glide type vehicles It is not intended that these results will reduce the need for dynamic loads analysis of new configurations, but it is hoped that design features that are beneficial for boost-glide vehicles from the loads standpoint can be pointed out

Only one iteration in the analysis of each case was carried out For example, load reductions due to a certain parameter change may permit a reduction of skin gage, thereby reducing structural weight and bending frequency In the second iteration these changes would be reflected in the dynamic loads calculation, and the trend established in the first iteration would be modified slightly However, for the purposes of the present study, trends established only by the first iterations were considered sufficiently accurate

The hypothetical boost-glide vehicle shown in Fig 1 was taken as the nominal configuration for the present study Since pitch-plane loads are more critical for vehicles having large winged payloads, only pitch-plane motions were considered, and wind profiles were assumed to lie in this plane The major parameters were varied one at a time, retaining the nominal values of all other parameters in most cases In some cases when a change in the parameter being studied resulted in a predictable change in another parameter, this change was implemented Parameters that were considered fixed quantities in the investigations were payload weight and the total stage weights The mission profile also was considered fixed except in the thrust to weight ratio variations

Unless specifically stated to the contrary, the attitude control law was used, with gains adjusted to maintain a pitch frequency and damping ratio of 0 5 cps and 0 6 critical throughout first stage boost

Parameters that were varied include length to diameter ratio, mass distribution, structural stiffness, payload lifting area, tailfin area, control law, and initial thrust to weight ratio Unless otherwise stated, wind shear loads were obtained by using a digital program to solve Eqs (1–16) for the response to the wind profile shown in Fig 2

Length to Diameter Ratio

Eight different configurations were analyzed, including the nominal configuration Variations from the nominal included changes in over-all length to diameter ratio and also changes in the first and second stage length to diameter ratios individually In these studies payload weight and lifting area and over-all weight and volume were held constant as length to diameter ratio (L/d) was varied

In varying over-all L/d, the nondimensional radius (r/r_{max}), skin thickness (t/t_{max}), and mass per unit length (m/m_{max}) were assumed to be the same functions of nondimensional length (x/L) for all fineness ratios Under these assumptions the mode shapes remained the same functions of x/L The bending frequencies were assumed to be inversely proportional to $(L/d)^{4/3}$, based on skin gage changes to maintain the same predicted stress in each configuration Pertinent data on each configuration analyzed are given in Table 2

In varying the individual stage length to diameter ratios, the nondimensional radii, skin thickness, and mass per unit length were not the same functions of x/L as the nominal configuration Consequently, new mode shapes had to be calculated for these configurations The configurations were 1)

Table 2 Over-all L/d variations

$\frac{(L/d)}{(L/d)_{n\ m}}$	L/d	L, in	D_1, in	D_2, in	$\omega_1^2/\omega_{1nom}^2$ (ω_{1nom} = 2 53 cps at t = 0)	2nd stage, EI/EI_{nom}	1st stage, EI/EI_{nom}
1 0	12 94	1709	132	108	1 0	1 0	1 0
0 5	6 47	1077	166 3	136 1	2 52	2 52	2 52
0 75	9 70	1411	145 2	118 9	1 468	1 468	1 468
1 4	18 11	2140	117 9	96 5	0 638	0 638	0 638

Table 3 Stage L/d variations

L/d	L, in	D_1, in	D_2, in	2nd stage EI/EI_{nom}	1st stage, EI/EI_{nom}
11 53	1499	132	132	1 0	1 0
14 43	1906	132	94 4	1 0	1 0
18 80	2032	108	108	1 0	1 0
8 82	1467 5	166 3	108	1 0	1 0

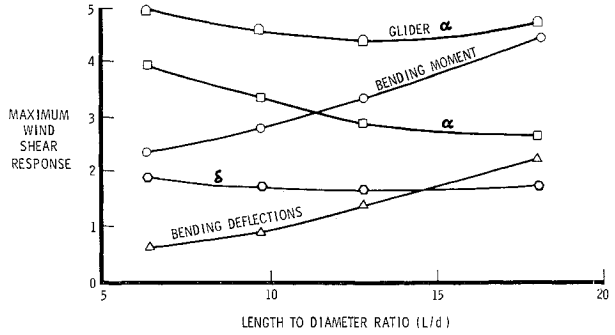

Fig 6 Influence of over-all L/d on maximum responses

second stage diameter increased to equal the first stage, 2) second stage L/d increased to 1 5 nominal, 3) first stage diameter reduced to equal the second stage, and 4) first stage L/d reduced to 0 5 nominal Pertinent data on these configurations are given in Table 3

Figure 6 shows the effect of over-all L/d on maximum wind-shear responses It is seen that maximum bending moment and bending deflection increase with increasing L/d Maximum rigid body angle of attack decreases, and maximum gimbal angle does not change significantly with L/d Angle of attack at the glider center of pressure is larger than the rigid body angle of attack because of bending deflections, and it increases slightly as the L/d becomes greater than nominal because of the increased bending deflection

Figure 7 shows the effect of changing length to diameter ratios of individual stages As seen in Fig 7, bending loads were more sensitive to changes in second stage L/d than to changes in first stage

Mass Distribution

Since the major portion of the vehicle mass is in the fuel and oxidizer, significant mass distribution changes imply a redistribution of fuel or oxidizer mass This was accomplished by placing the second stage liquid oxygen tank forward of the liquid hydrogen tank instead of aft Moving the second stage oxygen tank forward changed the center of gravity location, pitching moment of inertia, mode shapes, generalized masses, and bending frequencies

Figure 8 shows a comparison of the maximum wind-shear bending moment diagram with that of the nominal configuration It is seen that the change in mass distribution produced a large reduction in maximum bending moment Moving the heavy oxygen tank closer to the glider made the inertia load distribution more like the airload distribution Since the airload and inertia load were opposite in sign, the effect was to reduce the net load The increased bending frequency and more forward center of gravity of this configuration also may have helped to reduce the maximum load From the standpoint of wind-shear loads, it is always advantageous to distribute the mass in such a way that the inertia load distribution more closely approximates the airload distribution

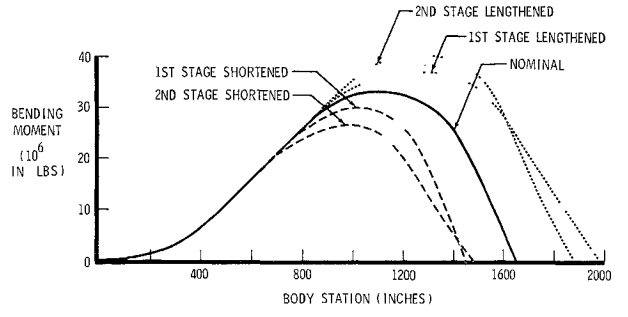

Fig 7 Influence of stage L/d changes on maximum wind-shear bending loads

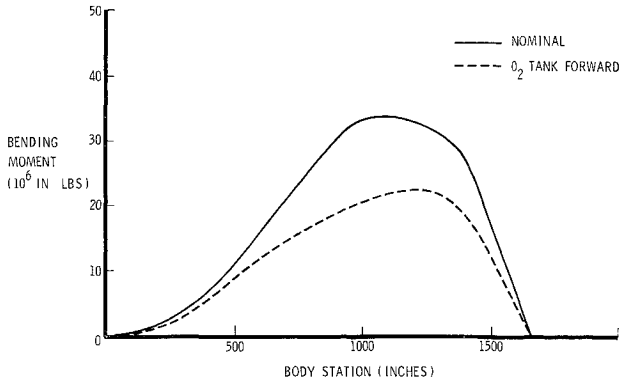

Fig 8 Effect of mass distribution change on maximum wind-shear bending loads

Structural Stiffness

Changes in over-all stiffness were accomplished by changing the structural frequencies, keeping the mode shapes and other parameters the same It was assumed that the structural weight changes were accompanied by equal and opposite changes in propellant weight Configurations having structural stiffness ratios of 0 5, 0 75, and 2 0 with respect to the nominal configuration were analyzed The results are shown in Fig 9, in which maximum wind-shear bending moment is plotted vs stiffness ratio It is seen that bending moments are sensitive to stiffness changes only in the reduced stiffness range The curve in Fig 9 has two asymptotes not shown: a horizontal one under the curve corresponding to the rigid body results and a vertical one to the left of the curve corresponding to the stiffness ratio at which aeroelastic instability would occur The vehicle was unstable for stiffness ratios less than 0 437

The deleterious effect of inadequate stiffness is readily apparent in Fig 9 Also indicated is the need for including structural flexibility effects in the loads analysis, since the actual loads for the flexible vehicle can be considerably larger than the loads predicted on the basis of a rigid body (infinite stiffness) analysis For very large boosters, stiffness requirements may be dictated not by loads considerations but by the necessity for adequate frequency separation between the rigid body and first bending frequencies to prevent instabilities arising from feedback of structural frequencies through the control system

Payload Lifting Area

For a given mission, the payload lifting area is usually a fixed constraint that cannot be varied to alleviate booster loads However, an indication of the magnitude of design changes needed to adapt a given boost system for use with winged payloads can be obtained by examining the effects of

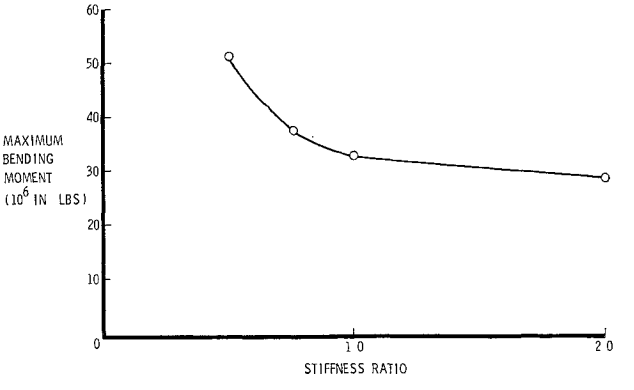

Fig 9 Influence of structural stiffness on maximum wind-shear bending loads

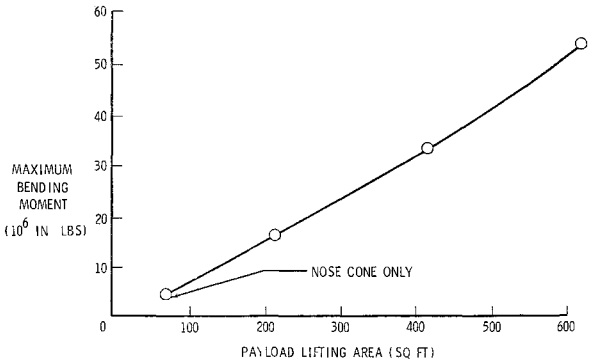

Fig 10 Influence of payload lifting area on maximum wind-shear bending moment

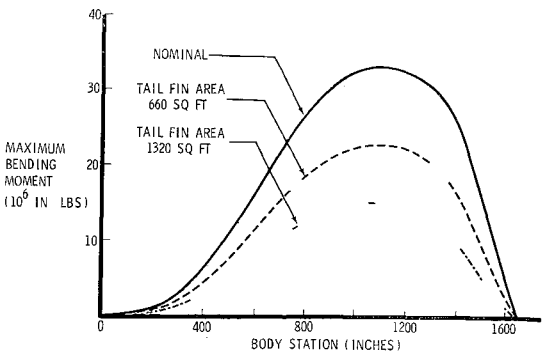

Fig 11 Influence of tail fin area on maximum wind-shear bending moments

variations in this parameter on wind-shear bending loads

Four configurations, including the nominal, were chosen Winged configurations of 210 ft², 420 ft² (nominal case), and 630 ft² lifting areas, plus a cone cylinder having no wing surfaces were analyzed The variation of normal force derivative with Mach number was assumed to be that of the nominal configuration, except for the cone cylinder for which momentum theory was used The stiffness and mass distributions were assumed to remain unchanged

The influence of payload lifting area on maximum wind-shear bending moments is shown in Fig 10 It is seen that bending loads are almost directly proportional to the lifting area Evidently, payload lifting area is one of the most significant parameters influencing dynamic loads Engine gimballing in response to wind shear was also greatly influenced by payload lifting area Maximum gimbal angles were 2 2°, 7 5°, 15 9°, and 25 6° for the configurations having the nose cone only, 210 ft², 420 ft², and 630 ft² areas, respectively It is probable that a major redesign would be required to adapt a booster designed for ballistic payloads to winged payloads

Variation of Tail Fin Area

Two finned configurations were analyzed In the first case the fins were sized to provide at least a small positive static stability margin throughout first stage boost, and in the second case the fin area was one-half that of the first The actual areas were 1320 and 660 ft²

Figure 11 shows a comparison of the maximum wind-shear bending moment diagrams with that of the nominal unfinned configuration Tail fins appear to be quite effective in reducing bending loads

In determining whether the over-all effect of these large fins is beneficial, one must compare their weight and drag losses with the weight saving made possible by the reduction in bending moments Such a comparison showed that the use of fins on this configuration is not advantageous when based on weight and performance considerations Performance losses due to the fins would have to be weighed against possible advantages of the fins One of these advantages might be reduction of engine gimballing requirements Maximum gimbal angles in response to the wind profile were 0 4°, 6 0°, and 15 9°, for the configurations with 1320 ft² fins, 660 ft² fins, and no fins, respectively Another advantage of the fins for a manned vehicle might be to reduce the pitch divergence rate in the event of a control system failure

Control Law

A comparison of the maximum bending moments predicted by the nonlinear solutions in Figs 3–5 shows that control law has a significant effect on wind-shear loads The bending moment was highest with the attitude control law, employing no angle of attack feedback, and lowest with the minimum drift law, employing the largest angle of attack feedback gain Apparently, the angle of attack feedback was very effective in alleviating wind-shear loads

In effect, the angle of attack feedback caused the vehicle to respond as if it had tail fins As shown in Fig 11, tail fins were very effective in reducing bending loads; but they increased the weight and drag There is virtually no weight penalty associated with the angle of attack feedback

Thrust to Weight Ratio

Mission profile changes were accomplished by varying the initial thrust to weight ratio (T_0/W_0) In each case a trajectory was determined to achieve the same first stage burnout flight path angle following a gravity turn Four values of T_0/W_0 were used: 1 25, 1 437 (nominal case), 1 80, and 2 20 The pertinent engine parameters in each case are given in Table 4

In determining the influence of these mission profile changes on wind-shear loads, several approaches were considered First, each T_0/W_0 case could have been subjected to the same wind profile, as was done in the other parameter studies, and the maximum bending moments compared This approach was rejected because the altitude of maximum sensitivity to wind shear changes when the mission profile is changed Another approach would be to use a single profile in each case, but to shift the altitude of the wind spike to the critical altitude in each case This approach was also rejected because of the difficulty in determining whether a change in response was due mainly to the mission profile change or the forcing function change The approach finally decided upon was to use a large sample of measured wind profiles as the environment and to fly all four T_0/W_0 configurations through this same environment Two hundred winter wind profiles measured over a 5 year period at Montgomery, Alabama, were the wind sample used The objective of the analysis was to compare the 1% bending moments experienced by each T_0/W_0 configuration in flying through this sample

Each of the four T_0/W_0 configurations was flown through the 200 Montgomery wind profiles using a digital program

Table 4 Engine parameters

T_0/W_0	T_0, lb	Weight rate of flow, lb/sec	Exit area, in ²	Burn time, sec
1 25	435,000	1740	4735	155 2
1 437	500 000	2000	5442	135
1 80	626,400	2505	6816	107 8
2 20	765 600	3062	8332	88 17

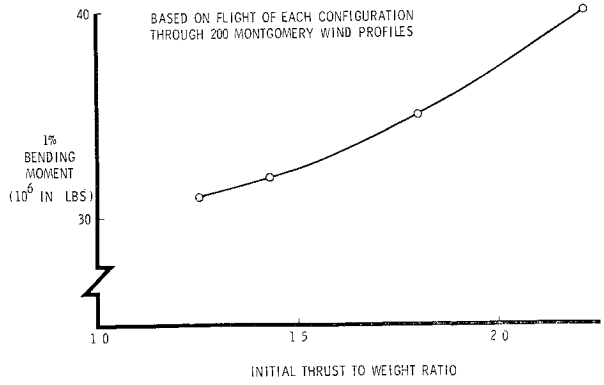

Fig 12 Influence of initial thrust to weight ratio on bending loads

based on the quasi-steady method previously described It was assumed that the vehicle was headed directly into the wind in each flight, and changes in wind direction with altitude were neglected Thus it was necessary to consider only pitch-plane motions The six or seven most severe wind profiles as identified by the quasi-steady analysis were then used as inputs for dynamic wind-shear loads analysis of each T_0/W_0 configuration, using a digital program to solve Eqs (1–16) The 1% bending moment for each configuration was determined by the method of Ref 2, i e , the high-load end of each load probability distribution curve was redefined using the six or seven maximum loads determined by the dynamic solutions, and the intersections of these redefined curves with the 1% probability level were noted The variation of 1% bending moment with T_0/W_0 is shown in Fig 12

Concluding Remarks

Methods for determining wind-shear loads during boosted flight were studied, and the influence of parameter variations on wind-shear loads on a boost-glide vehicle was determined Conclusions reached in the study of methods are applicable to boosted flight vehicles in general However, the results of the parameter variation studies should be applied with caution, since they are based on a family of configurations typifying only one class of vehicles The results are applicable specifically to medium sized boosters with winged payloads

In the study of analysis methods it was found that perturbation equations of motion, which treat all parameters as functions of time based on the nominal no wind trajectory, are less accurate for determining pitch-plane wind-shear loads than the nonlinear equations, in which a wind-disturbed trajectory is computed The accuracy of the quasi steady method examined in this study is greatly influenced by the control law The accuracy obtained ranged from good with the attitude control law to very poor with the minimum drift control law

In the parameter studies it was found that increasing fineness ratio, payload lifting area, and thrust to weight ratio tended to increase wind-shear bending loads, and that increasing structural stiffness, tailfin area, and angle of attack feedback gain tended to reduce loads Changing the mass distribution to make the inertia load more like the airload distribution also effectively reduced bending loads Payload lifting area was probably the most significant parameter influencing bending loads, and the use of a minimum drift control law appears to be the most attractive method of alleviating wind-shear loads on boost-glide type vehicles

References

[1] Clingan, B E , Gates, R M , and Andrews, J S , Dynamic loads during boosted flight," U S Air Force Systems Command, Aeronaut Systems Div TDR-63 302 (May 1963)

[2] Clingan, B E , 'A rapid method for determining wind shear design loads based on a set of measured profiles," Proc Natl Symp on Winds for Aerospace Vehicle Design, Vol II, Air Force Surveys in Geophys 140, Air Force Cambridge Res Lab 62 273 (II) (March 1962)

[3] Bohne, Q R , Clingan, B E , deCeault, C W , and Deutschle, P C, ' The dynamic response of advanced vehicles," Wright Air Dev Div TR 60 518 Wright Patterson Air Force Base, Ohio (September 1960)

[4] Hoelker, R F , "The principle of artificial stabilization of aerodynamically unstable missiles," U S Army Ballistic Missile Agency Rept DH-TR-64-59, Redstone Arsenal, Ala (September 1959); Confidential

[5] Clingan, B E , ' Dynamic analysis of wind shear and gust loads for advanced vehicles " Boeing Doc D2-10052, Seattle, Wash (July 1961)

[6] Sissenwine, N , "Revised 1% synthetic wind profile," Geophysics Res Directorate, Air Force Cambridge Res Lab Memo , Air Res Dev Command, U S Air Force, Laurence G Hanscom Field, Bedford, Mass (June, 1959)